Brain-wide neuronal activation and functional connectivity are modulated by prior exposure to repetitive learning episodes.

Dylan J. Terstege[1] Isabella M. Durante[1] & Jonathan R. Epp[1]*

[1]Department of Cell Biology and Anatomy, Hotchkiss Brain Institute, Cumming School of Medicine, University of Calgary, 3330 Hospital Drive NW, Calgary, Alberta, Canada T2N 4N1.

* Corresponding author

Dept. of Cell Biology & Anatomy

University of Calgary

HMRB 162, Health Sciences Centre

3330 Hospital Dr. NW

Calgary, AB

T2N 4N1

jonathan.epp1@ucalgary.ca

Conflict of Interest Statement

The authors declare no conflicts of interest.

Acknowledgements

Funding for this study was provided by The Brain Canada Foundation/The Azrieli Foundation Early Career Capacity Building Grant (4709) to JRE.

ABSTRACT

Memory storage and retrieval are shaped by past experiences. Prior learning and memory episodes have numerous impacts on brain structure from micro to macroscale. Previous experience with specific forms of learning increases the efficiency of future learning. It is less clear whether such practice effects on one type of memory might also have transferable effects to other forms of memory. Different forms of learning and memory rely on different brain-wide networks but there are many points of overlap in these networks. Enhanced structural or functional connectivity as a result of one type of learning may be transferable to another type of learning due to this overlap in memory networks. Here, we investigated the impact of prior chronic spatial training on the task-specific functional connectivity related to subsequent contextual fear memory recall in mice. Our results show that mice exposed to prior spatial training exhibited decreased brain-wide activation compared to control mice during the retrieval of a context fear memory. With respect to functional connectivity, we observed changes in several network measures notably an increase in global efficiency. Interestingly, we also observed an increase in network resilience based on simulated targeted node deletion. Overall this study suggests that chronic learning has transferable effects on the functional connectivity networks of other types of learning and memory. The generalized enhancements in network efficiency and resilience suggest that learning itself may protect brain networks against deterioration.

Introduction

It has been well established that prior learning experiences alter the canvas against which new learning occurs. Learning results in numerous structural changes in the brain ranging from cellular and synaptic changes (Lendvai et al., 2000; Nyberg et al., 2003; Holtmaat et al., 2005; De Paola et al., 2006; Epp et al., 2013) to altered macroscale measurements or regional size and shape (Maguire et al., 2003; Draganski et al., 2004; Bermudez et al., 2008; Hyde et al., 2009; Scholz et al., 2009). A classic example of learning-induced structural changes is the change in hippocampal volume that occurs as a result of intense practice with spatial navigation such as in London taxi drivers (Maguire et al., 2000). Similar increases in hippocampal volume have also been observed in mice that were trained on a spatial learning task (Lerch et al., 2011).

To the extent that there are relationships between brain function and underlying structure, it should be predicted that learning-induced structural changes should also induce functional changes. Training-induced increases in hippocampal volume for example are also associated with enhanced memory performance (Bohbot et al., 2007).

In addition to structural changes, learning has been shown in some studies to change the organization of memories in the brain. In rats, previous studies have indicated that prior training with a memory task can prevent lesion-induced deficits in both similar and slightly distinct memory tasks (Clark and Delay, 1991; Ocampo et al., 2018). This suggested that prior learning experiences fundamentally change how and where future memories are encoded (Owen et al., 2010; Nouchi et al., 2012; West et al., 2017). Experiments such as these suggest some form of reorganization but do not give a complete picture as to how this reorganization has occurred.

Functional imaging experiments in humans have provided evidence that cognitive stimulation, or memory training, alter brain functional connectivity (Martínez et al., 2013; Dresler et al., 2017; Bagarinao et al., 2019; Miró-Padilla et al., 2019; Finc et al., 2020). These findings are of significant importance because reorganization of functional networks could increase the efficiency of learning and memory and could even increase the resilience of cognitive processes to damage or deterioration. However, investigating the influence of prior learning on altered functional connectivity

in humans is complicated by the diverse cognitive, genetic and lifestyle differences in different individuals.

In the present study, to further elucidate the impact of prior learning on memory related functional connectivity, we have developed a mouse model in which mice are trained in a repeated acquisition spatial learning and memory task for several months. Using mice, we are able to control for environmental and genetic factors, and we can also control for prior learning experiences. Our aim was to investigate whether learning one task (spatial learning) would increase the efficiency of the functional networks underlying a different form of memory (contextual fear memory). To do so we adopted a brain-wide functional connectivity approach using immediate early gene imaging that has been recently described (Wheeler et al., 2013; Vetere et al., 2017; Scott et al., 2020).

In this study, we show that chronic cognitive stimulation, in the form of spatial learning is sufficient to induce generalized changes in the organization of functional connectivity networks underlying a test of contextual fear memory.

Methods

Mice:

8-week-old male C57BL/6J mice purchased from The Jackson Laboratory (Bar Harbour, ME, United States) were used for all experiments. Upon arrival, mice were group housed, 3-4 mice per cage, under a 12-h light/12-h dark cycle with *ad libitum* access to food and water. Behavioural tests and network analyses were conducted using groups of $n = 6$. All procedures were conducted in accordance with protocols approved by the University of Calgary, Health Sciences Animal Care Committee, following the guidelines of the Canadian Council for Animal Care.

Morris Water Task Training:

In order to provide mice with chronic cognitive stimulation, we trained half of the mice on a repeated acquisition and performance testing variant of the Morris Water Task (MWT) (Spanswick et al., 2007). In this version of the task, the hidden escape platform is

moved every second day which required the mice to repeatedly acquire new spatial memories throughout a 10-week training period. We used 10 different platform locations, with each platform location occurring on 2 separate occasions. Mice were trained 4 days per week (2 platform locations). During each daily session, mice were given four trials. Each trial lasted a maximum of 60 seconds and was initiated by placing the mouse gently into the pool, facing the wall. The start location was from a different cardinal compass position around the pool for each trial and the order of start locations was randomized each day. Trials were terminated once the mouse located the hidden platform. If the platform was not found after 60 seconds, mice were gently guided to the platform by the experimenter. Once on the platform, mice were given 15 seconds to remain on the platform before being returned to their cage. Trials were interleaved, whereby each mouse performed their first trial before the first mouse performed its second of four daily trials. This resulted in an intertrial interval of approximately 10 minutes. The circular pool had a diameter of 150 cm and a depth of 50 cm. The pool was filled so that the water level was 2 cm above the surface of a circular escape platform that had a diameter of 11 cm. The water was made opaque using white non-toxic tempera paint. The water was kept at a constant temperature of 22°C and stirred and cleaned of debris before each trial. Automated tracking software (ANY-Maze, Stoelting, Wood Dale, IL, United States) was used to record and analyze swim behaviours in the pool, including swim speed, distance travelled and latency to locate the hidden platform.

Contextual Fear Conditioning:

After the conclusion of the Morris Water Task training protocol, all mice were trained in contextual fear conditioning. Training was conducted in sound-attenuated chambers with grated floors through which shocks (0.5 mA; 2 s) were delivered (Ugo Basile, Gemonio, Italy). Mice were first allowed to acclimate to the chamber for 2 minutes prior to the presentation of a series of 3 shocks, each separated by an interval of 90 seconds. 24 h after the training session, mice were returned to the conditioning chambers for a 6-min retention test. During this test, no shocks were administered, and behaviour was monitored via an overhead infrared camera in conjunction with an automated tracking

software (ANY-Maze, Stoelting, Wood Dale, IL, United States). The chamber was cleaned using 70% ethanol and allowed to dry before and after each trial.

Perfusions and Histology:

Mice were transcardially perfused with 0.1 M phosphate buffered saline (PBS) followed by 4% formaldehyde 90 minutes after retention testing. Brains were then extracted and postfixed in 4% formaldehyde for 24 h. Fixed brains were cryoprotected in 30% W/V sucrose solution at 4°C until no longer buoyant. From cryoprotected brains, serial coronal sections with a thickness of 40 µm were cut on a cryostat (Leica Biosystems, Concord, ON, Canada) and stored in 12 series at -20°C in antifreeze solution.

Immunohistochemistry:

Tissue sections were washed 3 times (10 minutes per wash) in 0.1M PBS before being incubated in a primary antibody solution of 1:2000 rabbit anti-c-Fos primary antibody (226 003, Synaptic Systems, Göttingen, Germany), 3% normal donkey serum, and 0.03% Triton-X100 for 48 h at room temperature on a tissue shaker. Tissue sections were washed 3 x 10 minutes in 0.1M PBS before secondary antibody incubation. The secondary antibody solution was composed of 1:500 donkey anti-rabbit Alexa Fluor 488 (111-545-003, Cedar Lane Labs, Burlington, ON, Canada) in PBS for 24 h at room temperature. Sections were then transferred to 1:2000 DAPI solution for 15 min before being washed 3 x 10 minutes in 0.1M PBS. Labeled sections were mounted to glass slides and coverslipped with PVA-DABCO mounting medium.

Brain-Wide c-Fos Quantification:

Quantification of fluorescent c-Fos labeled cells was conducted using a custom semi-automated segmentation and registration pipeline (Figure 2A). Slides were first imaged using an Olympus VS120-L100-W slide scanning microscope (Richmond Hill, ON, Canada). Images were collected using a 10x objective with a numerical aperture of 0.40 and a Hamamatsu ORCA-Flash4.0 camera. Labelled c-Fos was imaged using a FITC filter cube and a 9.00 V lamp at an intensity of 100% and an exposure time of 140 ms. DAPI staining was imaged under the same conditions, but with a DAPI filter cube

and an exposure time of 65 ms. Cells expressing a c-Fos label were segmented using the machine learning-based pixel and object classification program, *Ilastik* (Berg et al., 2019). To further prepare *Ilastik* output images and DAPI channel photomicrographs for regional registration, a custom plug-in was written for *ImageJ*. The pixel intensity threshold of the *Ilastik* outputs was adjusted so as to only contain objects which the program determined to be within the correct range of pixel intensities and shapes. To compensate for inadequate regional area measurements at an image-by-image level in the atlas registration software, a mask of evenly spaced binary points was generated from the DAPI channel image. The pixel intensity thresholds of these images were adjusted to create a binary mask in the shape of the tissue section. Grid lines were then overlaid to create a mask of binary points arranged in a square grid in the shape of the tissue section. Adjacent binary points were spaced by 22 μm, therefore, each point in the mask accounted for an area of 484 μm^2.

Next, tissue sections were registered to plates of the *Allen Mouse Brain Atlas* using the *R*-based *Whole Brain* software (Fürth et al., 2018). Using this software, DAPI channel images were used as references to which the atlas plates were aligned. The number of segmented c-Fos labeled cells per neuroanatomical region was quantified in Whole Brain. Similarly, the binary point masks were processed to count the number of points in each region. Regional areas were then approximated using a Cavalieri-based point counting approach, whereby the number of mask points in each region was multiplied by the area accounted for by each point. This allowed for the c-Fos labeled cells to be normalized by area and presented as regional cell densities.

Validation of c-Fos Quantification and Regional Area Approximation:

A separate cohort of mice was used for the validation of c-Fos labeled cell segmentation and regional area approximation. c-Fos immunostaining and imaging was identical to the methods described previously. To generate ground truth cell counts as a gold standard for our automated counting procedure, ten 500 μm x 500 μm Regions of interest (ROI) were randomly generated from each of several regions including the basolateral amygdala, CA1, dentate gyrus, paraventricular nucleus, and the

retrosplenial cortex. These ROIs were processed through our *Ilastik* label segmentation pipeline (representative raw and processed images in Figure 2B). In addition, the same ROIs were hand counted independently by 4 experimenters blind to the automated cell count results. The total numbers of cells counted across all counting boxes were then compared to assess whether or not *Ilastik* could segment fluorescent c-Fos labels within natural and acceptable inter-rater variability.

To assess the accuracy of regional area approximations, areas generated using the Cavalieri-based point counting approach were compared to the areas of these same regions which were manually traced in *ImageJ*. During this analysis, five photomicrographs of each of the following regions were examined: basolateral amygdala, CA1, dentate gyrus, paraventricular nucleus, and the retrosplenial cortex.

Functional Connectivity Network Generation:

We focused on a selection of 98 regions based on our ability to consistently and reliably discriminate these regions using a DAPI stained image as reference (see Supplemental Table 1 for list of regions and abbreviations). From this list of regions, c-Fos label densities were cross correlated within each group to generate pairwise correlation matrices. Correlations were filtered by statistical significance (alpha = 0.05) and a false discovery rate of 95%. For network analyses, correlation matrices were binarized to adjacency matrices using a Pearson's *r threshold* $r \geq 0.80$. To analyze adjacency matrices as network graphs, neuroanatomical regions are plotted as nodes. Connections were drawn between nodes whereby correlations surpassed correlation matrix thresholding parameters.

Functional Connectivity Network Analysis:

Graph theoretical analyses were applied to network graphs to examine global and local properties of the network. These analyses were guided by the use of the *Brain Connectivity Toolkit* (Rubinov and Sporns, 2010) and other custom analyses. Network properties examined include *connection strength*, *node degree*, *network density*, *global efficiency*, *betweenness centrality*, *Katz centrality*, and *network resiliency*. In the following definitions, N is the array of nodes in the network represented by adjacency

matrix *A*. The number of nodes in the network is represented by *n* and the number of connections between nodes is *l*. The variable a_{ij} is the index into the adjacency matrix which indicates the connection status of nodes *i* and *j*. The presence of a connection is represented by $a_{ij} \neq 0$ (Rubinov and Sporns, 2010).

Connection strength was assessed by examining the magnitude of the Pearson correlation coefficient between the c-Fos densities of a pair of regions. For this analysis, correlations were only filtered by statistical significance at $\alpha = 0.05$ and a false discovery rate of 95%. All correlations which met these conditions were considered.

Node degree is the number of connections that link a node to the rest of the network (Rubinov and Sporns, 2010).

$$k_i = \sum_{j \in N} a_{ij}$$

Network density is a metric of network dispersion. It is expressed as a proportion of the number of connections in a given network over the number of connections which would be required to saturate a network of the same size (Rubinov and Sporns, 2010).

$$k_{den} = \frac{2l}{n^2 - n}$$

Global efficiency is defined as the inverse of the average shortest path of connections between all possible pairs of nodes (Latora and Marchiori, 2001; Achard and Bullmore, 2007; Rubinov and Sporns, 2010).

$$E = \frac{1}{n} \sum_{i \in N} \frac{\sum_{j,h \in N, j \neq i} {d_{ij}}^{-1}}{n - 1}$$

Betweenness centrality and *Katz centrality* are measures which can be used to assess the importance of a node in the effective communication of a network. *Betweenness centrality* quantifies the number of shortest paths between nodes that pass-through a given node (Freeman, 1978; Brandes, 2001; Rubinov and Sporns, 2010).

$$b_i = \frac{1}{(n-1)(n-2)} \sum_{\substack{h,j \in N \\ h \neq j, h \neq i, j \neq i}} \frac{\rho_{hj}(i)}{\rho_{hj}}$$

Katz centrality applies an eigenvector approach to this metric by weighting the connections involving more highly connected nodes more heavily than those from lesser connected nodes when considering the makeup of the shortest paths which pass through a given node (Katz, 1953; Hubbell, 1965). The attenuation factor, α, used for this analysis was 0.1 (Zhan et al., 2017).

$$C_{Katz,i} = \sum_{k=1}^{\infty} \sum_{j=1}^{n} \alpha^k (A^k)_{ij}$$

Network resiliency was assessed through targeted node deletion and an assessment of the size of the largest community of connected nodes and global network efficiency with each deletion. Nodes were targeted for deletion in decreasing order, from nodes with the highest degree to those with the lowest. Degree was recalculated after each deletion and the list was reordered accordingly.

Network metrics were both compared across conditions as well as used to assess small world-like network properties compared to random control network topology. Small world network distribution can be described as being efficient at both local and global scales (Watts and Strogatz, 1998). Random null control networks were generated for both the cognitive training and control groups and were matched for network size and degree distribution. Local efficiency was assessed by comparing mean clustering coefficients, while global efficiency was assessed by comparing bootstrapped global efficiency values with one hundred replacements.

<u>Statistical Analyses:</u>

All statistical tests for comparing behavioural data in the Morris Water Maze and contextual conditioning task, c-Fos segmentation and regional area approximation validation, and functional connectivity metric networks were conducted using GraphPad

Prism (GraphPad Software, San Diego California US). The generation of network metrics was conducted using MATLAB and R. Figures were generated using MATLAB, Cytoscape, and GraphPad Prism.

Results

Morris Water Maze Training Alters Memory Performance in Unrelated Tasks

To assess the generalization of improved cognitive performance following long-term spatial learning (Figure 1A-C), mice were trained and tested in a contextual fear conditioning paradigm (Figure 1D). The percentage of time that mice exhibited freezing behaviour was compared between groups and across the training and retention test sessions. Across both sessions, there were no significant differences in freezing behaviour (Figure 1E). However, when the retention was divided into a first half and a second half, mice who had received cognitive training displayed increased freezing behaviour during the first half of the test and then decreased freezing during the second half of the test, relative to control mice (Figure 1F) which may be indicative of changes in memory strength and/or behavioural flexibility.

Validation of c-Fos Segmentation and Neuroanatomical Atlas Registration

To assess the reliability of the semi-automated segmentation and registration pipeline used in this study (Figure 2A), we compared c-Fos counts obtained using this pipeline to those gathered manually (see representative images Figure 2B). We found that the number of c-Fos labeled cells quantified using *Ilastik* processing fell within the range of values counted manually by four different experimenters across a subset of regions with varying levels of background autofluorescence ($F_{1,15}$=0.09515, P=0.7620; Figure 2C). The inter-rater reliability was determined to be 15% across the datasets as a whole and the semi-automated cell counts were within 3.75% of the average of the manual cell counts. Manual and automated cell counts were highly correlated (*Pearson* r=0.9610, P<0.01) across the sampled brain regions (Figure 2D). *WholeBrain* region registration also produced regional area approximations that correlated highly (*Pearson* r=0.9941, P=<0.0001) with hand-traced regional area values (Figure 2E).

Prior spatial learning alters c-Fos expression associated with context memory recall.
We quantified regional c-Fos expression density in all 98 regions of interest. This is depicted in Figure 2F as the percent change from the control condition with long-term spatial learning. Interestingly, we observed a decrease in c-Fos expression density in approximately 87% of regions in mice that had received prior spatial training. A relatively small subset of regions showed an increase in c-Fos expression compared to control mice. With respect to brain-wide activity, prior spatial training resulted in an overall significant decrease (p=0.0123) in c-Fos expression (Supplemental Figure S1).

Morris Water Maze Training Alters Functional Connectivity Network Topology
Analyses of cross-correlated regional c-Fos expression density revealed differences in global functional connectivity network topology. On a global scale, we observed a reorganization of connections throughout the brain (Figure 3A-D). Relative to control conditions, mice that underwent prior cognitive training exhibited an increase in the overall density of functional connections during subsequent contextual fear memory retrieval (Figure 3E). Furthermore, there was a shift in the distribution of correlation strengths in mice that underwent long-term spatial learning (Pearson Threshold × Treatment interaction: $F_{3,776}$=3.904, P=0.0088). Relative to control mice, there was a significant increase in the proportion of regions that had Pearson correlation coefficients greater than 0.8 (P=0.0140; Figure 3F).

Control and Morris Water Maze Training Networks Exhibit Small-World Qualities
Functional connectivity networks in the brain are considered to be complex networks. Many complex networks exhibit small world organization. Small-world networks balance global efficiency with local clustering by having a small proportion of nodes to contribute disproportionately to the overall connectivity of the network (Watts and Strogatz, 1998; Bassett et al., 2006; Sporns and Honey, 2006). This type of organization facilitates specialized processing in dense, local clusters and efficient information transfer between clusters. Small world organization can be identified in networks with a heavy-tailed degree distribution and increased local clustering without compromising global

efficiency. Both networks from control and spatial learning groups exhibited this heavy-tailed degree distribution, with the majority of nodes making very few connections and a lesser number of nodes carrying disproportionate importance to the overall connectivity of the network (Figure 4A) (Bassett et al., 2006; Bullmore and Sporns, 2009)

Additional small-world properties based on clustering and efficiency were assessed by comparing functional connectivity networks to randomly generated control networks. These randomly generated networks were matched for size and degree distribution (Rubinov and Sporns, 2010). The random networks demonstrate the extent to which clustering would be expected in a network based purely on chance alone (Sporns, 2018). This then indicates that differences in topological characteristics between observed biological networks and the random null models are core to the behaviour of the biological networks (Betzel et al., 2016). Interpretations of comparisons to randomly generated null networks must consider that random networks have low mean clustering, which is associated with low local efficiency. However, while random network organization yields a low mean clustering coefficient, they also are characterized by having short mean path lengths, which is reflected in a high global efficiency (Watts and Strogatz, 1998).

Comparisons to random null networks highlighted that both the control and spatial learning networks showed increased clustering (Figure 4B) while maintaining the high global efficiency ($F_{1,388}$=178.6, P<0.0001) characteristic of random networks (Figure 4C). Together, these analyses indicate that the functional connectivity networks engaged during memory recall in both the control and spatial learning conditions exhibit properties that are consistent with small-world topology.

<u>Morris Water Maze Training Alters Cluster Organization and Connectivity.</u>
Observed changes in network topology extend to a local level. The organization of local communities within global networks changes with long-term spatial learning. While metrics such as the size of the giant component (GC) (Figure 5A-C), the number of components in the network (5D) and the mean size of each component (5E) undergo very little change with MWT training, differences arise in the connectivity patterns within these components (P=0.6226). Within the GC, MWT training increases the mean

number of connections per node (*P*=0.0215; 5F). The changes in connectivity also yield changes in network resiliency. When faced targeted deletion of nodes, in order of decreasing connectivity, long-term spatial learning increased the ability of the network to preserve its global efficiency (Figure 5G) and giant component size (Figure 5H).

Coinciding with these changes in network resiliency were changes in Katz centrality. Katz centrality is a measure of centrality which differentially weighs connections based on the degrees of the nodes involved (Katz, 1953). This measure has previously been shown to correlate highly with neuronal activity compared to other measures of centrality (Fletcher and Wennekers, 2018). While most nodes in the control network had similar Katz centrality vectors (Figure 5I), MWT training increased the centrality of a subset of regions (Figure 5J). There was considerable overlap between these regions with increased Katz centrality and the regions in the most densely connected region of the GC. This was further corroborated by analysis of regional degree distribution (Supplemental Figure S2C), which further highlighted an increase in connectivity of numerous amygdala subregions following spatial learning.

Discussion

In the current study we employed a brain-wide activity mapping approach to examine the impact of a prolonged period of repeated spatial learning on brain-wide patterns of activation and functional connectivity. We posited, that repeated activation of the circuits underlying spatial learning and memory might alter the networks that represent other forms of hippocampus dependent memory in the future. Our results clearly indicate that this prior spatial learning manipulation caused significant changes to the task-related functional connectivity associated with retrieval of a contextual fear memory.

We were most interested in investigating whether such a manipulation, which, might be viewed as memory practice or training, would enhance measures of efficiency when examining the storage and retrieval of future memories. We show here that the efficiency of brain-wide activation, as measured by c-Fos expression is greatly increased in the mice that had prior spatial training. Efficiency can be defined as equal or greater memory performance with the expenditure of fewer resources (i.e., a

decrease in activation). Our results show that contextual memory retrieval following spatial learning was associated with a decrease in the total c-Fos expressing cells throughout the brain compared to mice that had not previously experienced any spatial training. When examining this activation regionally we observed that approximately 87% of brain regions exhibited reduced activity, with the remainder showing an increase. This pattern of activity perhaps indicates that the behavioural expression of the memory retrieval is reliant on a smaller number of brain regions.

At a network level, global efficiency can be estimated as the inverse of the average shortest path lengths between all network nodes. This measure represents the relative ease or difficulty of integrating information across network nodes. Using this measure, we found that mice which had received prior spatial training exhibited enhanced global efficiency compared to controls during subsequent contextual memory retrieval. This analysis corroborates the increased efficiency based on overall brain activation. Further corroborating the increased efficiency are changes in the Katz centrality of the nodes within these networks. Centrality measures can be used as proxies of the relative importance of a node in effective communication across a network. Without prior spatial training, there was very little variability in the centrality of each node. However, similar to the changes in c-Fos expression density, spatial training greatly increased the centrality of a small subset of nodes. This distribution suggests that this subset of regions is relatively more important to the behavioural expression of the fear memory. Comparatively, in untrained mice the majority of regions are of very similar importance in the expression of this same behaviour.

Regardless of prior spatial training exposure, the networks engaged by contextual memory retrieval displayed characteristic small-world properties. Compared to random networks, we observed that the memory networks had a small number of highly connected regions, an increase in clustering coefficient, and equivalent global efficiency. We used Markov chain clustering to detect community structure within the networks. In both networks there was a large interconnected central component that did not change in size as a result of prior spatial training. However, there was a significant change in the density of connections in this community. This likely also enhanced the efficiency, a hypothesis which was supported by changes in network

resiliency. We applied targeted node deletion to the networks and noted that mice which had prior spatial training were able to retain a higher percentage of their basal global efficiency and the size of the largest central component. The densely connected community at the core of the network underlying fear memory expression in mice with prior spatial training contained many redundant connections. Therefore, more successive deletions were required to break apart communities. In being more resistant to targeted attack, this network can be said to be more resilient than the network obtained from control mice (Achard et al., 2006).

Increased resiliency to targeted node deletion presents interesting possibilities from the perspective of neurodegenerative disease. The pathology of many neurodegenerative conditions does not arise uniformly throughout the brain and rather targets the most highly involved regions of a network (Crossley et al., 2014). An efficient network which is more resilient to targeted attack has the potential to delay or reduce cognitive decline during early neurodegenerative disease progression (Rittman et al., 2019). Therefore, the potential exists for prior exposure to repetitive learning experiences to increase resiliency to deterioration.

References:

Achard S, Bullmore E (2007) Efficiency and cost of economical brain functional networks. PLoS Comput Biol 3:e17.

Achard S, Salvador R, Whitcher B, Suckling J, Bullmore E (2006) A resilient, low-frequency, small-world human brain functional network with highly connected association cortical hubs. J Neurosci 26:63–72.

Bagarinao E et al. (2019) Reorganization of brain networks and its association with general cognitive performance over the adult lifespan. Sci Rep 9:11352.

Bassett DS, Meyer-Lindenberg A, Achard S, Duke T, Bullmore E (2006) Adaptive reconfiguration of fractal small-world human brain functional networks. Proc Natl Acad Sci U S A 103:19518–19523.

Berg S, Kutra D, Kroeger T, Straehle CN, Kausler BX, Haubold C, Schiegg M, Ales J, Beier T, Rudy M, Eren K, Cervantes JI, Xu B, Beuttenmueller F, Wolny A, Zhang C, Koethe U, Hamprecht FA, Kreshuk A (2019) ilastik: interactive machine learning for (bio)image analysis. Nat Methods 16:1226–1232.

Bermudez P, Lerch JP, Evans AC, Zatorre RJ (2008) Neuroanatomical Correlates of Musicianship as Revealed by Cortical Thickness and Voxel-Based Morphometry. Cereb Cortex 19:1583–1596.

Betzel RF, Avena-Koenigsberger A, Goñi J, He Y, de Reus MA, Griffa A, Vértes PE, Mišic B, Thiran J-P, Hagmann P, van den Heuvel M, Zuo X-N, Bullmore ET, Sporns O (2016) Generative models of the human connectome. Neuroimage 124:1054–1064.

Bohbot VD, Lerch J, Thorndycraft B, Iaria G, Zijdenbos AP (2007) Gray matter differences correlate with spontaneous strategies in a human virtual navigation task. J Neurosci 27:10078–10083.

Brandes U (2001) A faster algorithm for betweenness centrality. J Math Sociol 25:163–177.

Bullmore E, Sporns O (2009) Complex brain networks: graph theoretical analysis of structural and functional systems. Nat Rev Neurosci 10:186–198.

Clark RE, Delay ER (1991) Reduction of lesion-induced deficits in visual reversal learning following cross-modal training. Restor Neurol Neurosci 3:247–255.

Crossley NA, Mechelli A, Scott J, Carletti F, Fox PT, McGuire P, Bullmore ET (2014) The hubs of the human connectome are generally implicated in the anatomy of brain disorders. Brain 137:2382–2395.

De Paola V, Holtmaat A, Knott G, Song S, Wilbrecht L, Caroni P, Svoboda K (2006) Cell type-specific structural plasticity of axonal branches and boutons in the adult neocortex. Neuron 49:861–875.

Draganski B, Gaser C, Busch V, Schuierer G, Bogdahn U, May A (2004) Changes in grey matter induced by training. Nature 427:311–312.

Dresler M, Shirer WR, Konrad BN, Müller NCJ, Wagner IC, Fernández G, Czisch M, Greicius MD (2017) Mnemonic Training Reshapes Brain Networks to Support Superior Memory. Neuron 93:1227-1235.e6.

Epp JR, Chow C, Galea LAM (2013) Hippocampus-dependent learning influences hippocampal neurogenesis. Front Neurosci 7:57.

Finc K, Bonna K, He X, Lydon-Staley DM, Kühn S, Duch W, Bassett DS (2020) Dynamic reconfiguration of functional brain networks during working memory training. Nat Commun 11:2435.

Fletcher JM, Wennekers T (2018) From Structure to Activity: Using Centrality Measures to Predict Neuronal Activity. Int J Neural Syst 28:1750013.

Freeman LC (1978) Centrality in social networks conceptual clarification. Soc Networks 1:215–239.

Fürth D, Vaissière T, Tzortzi O, Xuan Y, Märtin A, Lazaridis I, Spigolon G, Fisone G, Tomer R, Deisseroth K, Carlén M, Miller CA, Rumbaugh G, Meletis K (2018) An interactive framework for whole-brain maps at cellular resolution. Nat Neurosci 21:139–149.

Holtmaat AJGD, Trachtenberg JT, Wilbrecht L, Shepherd GM, Zhang X, Knott GW, Svoboda K (2005) Transient and persistent dendritic spines in the neocortex in vivo. Neuron 45:279–291.

Hubbell CH (1965) An Input-Output Approach to Clique Identification. Sociometry 28:377–399.

Hyde KL, Lerch J, Norton A, Forgeard M, Winner E, Evans AC, Schlaug G (2009) Musical training shapes structural brain development. J Neurosci 29:3019–3025.

Katz L (1953) A New Status Index Derived From Sociometric Analysis. Psychometrika 18:39–43.

Latora V, Marchiori M (2001) Efficient behavior of small-world networks. Phys Rev Lett 87:198701.

Lendvai B, Stern EA, Chen B, Svoboda K (2000) Experience-dependent plasticity of dendritic spines in the developing rat barrel cortex in vivo. Nature 241404:876–881.

Lerch JP, Yiu AP, Martinez-Canabal A, Pekar T, Bohbot VD, Frankland PW, Henkelman RM, Josselyn SA, Sled JG (2011) Maze training in mice induces MRI-detectable brain shape changes specific to the type of learning. Neuroimage 54:2086–2095.

Maguire EA, Gadian DG, Johnsrude IS, Good CD, Ashburner J, Frackowiak RS, Frith CD (2000) Navigation-related structural change in the hippocampi of taxi drivers. Proc Natl Acad Sci U S A 97:4398–4403.

Maguire EA, Spiers HJ, Good CD, Hartley T, Frackowiak RSJ, Burgess N (2003) Navigation expertise and the human hippocampus: a structural brain imaging analysis. Hippocampus 13:250–259.

Martínez K, Solana AB, Burgaleta M, Hernández-Tamames JA, Alvarez-Linera J, Román FJ, Alfayate E, Privado J, Escorial S, Quiroga MA, Karama S, Bellec P, Colom R (2013) Changes in resting-state functionally connected parietofrontal networks after videogame practice: Videogame Practice and Functional Connectivity. Hum Brain Mapp 34:3143–3157.

Miró-Padilla A, Bueichekú E, Ventura-Campos N, Flores-Compañ M-J, Parcet MA, Ávila C (2019) Long-term brain effects of N-back training: an fMRI study. Brain Imaging Behav 13:1115–1127.

Nouchi R, Taki Y, Takeuchi H, Hashizume H, Akitsuki Y, Shigemune Y, Sekiguchi A, Kotozaki Y, Tsukiura T, Yomogida Y, Kawashima R (2012) Brain training game improves executive functions and processing speed in the elderly: a randomized controlled trial. PLoS One 7:e29676.

Nyberg L, Sandblom J, Jones S, Neely AS, Petersson KM, Ingvar M, Bäckman L (2003) Neural correlates of training-related memory improvement in adulthood and aging. Proc Natl Acad Sci U S A 100:13728–13733.

Ocampo AC, Squire LR, Clark RE (2018) The beneficial effect of prior experience on the acquisition of spatial memory in rats with CA1, but not large hippocampal lesions: a possible role for schema formation. Learn Mem 25:115–121.

Owen AM, Hampshire A, Grahn JA, Stenton R, Dajani S, Burns AS, Howard RJ, Ballard CG (2010) Putting brain training to the test. Nature 465:775–778.

Rittman T, Borchert R, Jones S, van Swieten J, Borroni B, Galimberti D, Masellis M, Tartaglia MC, Graff C, Tagliavini F, Frisoni GB, Laforce R Jr, Finger E, Mendonça A, Sorbi S, Rohrer JD, Rowe JB, Genetic Frontotemporal Dementia Initiative (GENFI) (2019) Functional network resilience to pathology in presymptomatic genetic frontotemporal dementia. Neurobiol Aging 77:169–177.

Rubinov M, Sporns O (2010) Complex network measures of brain connectivity: uses and interpretations. Neuroimage 52:1059–1069.

Scholz J, Klein MC, Behrens TEJ, Johansen-Berg H (2009) Training induces changes in white-matter architecture. Nat Neurosci 12:1370–1371.

Scott GA, Terstege DJ, Vu AP, Law S, Evans A, Epp JR (2020) Disrupted Neurogenesis in Germ-Free Mice: Effects of Age and Sex. Front Cell Dev Biol 8:407.

Spanswick SC, Epp JR, Keith JR, Sutherland RJ (2007) Adrenalectomy-induced granule cell degeneration in the hippocampus causes spatial memory deficits that are not reversed by chronic treatment with corticosterone or fluoxetine. Hippocampus 17:137–146.

Sporns O (2018) Graph theory methods: applications in brain networks. Dialogues Clin Neurosci 20:111–121.

Sporns O, Honey CJ (2006) Small worlds inside big brains. Proc Natl Acad Sci U S A 103:19219–19220.

Vetere G, Kenney JW, Tran LM, Xia F, Steadman PE, Parkinson J, Josselyn SA, Frankland PW (2017) Chemogenetic Interrogation of a Brain-wide Fear Memory Network in Mice. Neuron 94:363-374.e4.

Watts DJ, Strogatz SH (1998) Collective dynamics of “small-world” networks. Nature 393:440–442.

West GL, Zendel BR, Konishi K, Benady-Chorney J, Bohbot VD, Peretz I, Belleville S (2017) Playing Super Mario 64 increases hippocampal grey matter in older adults. PLoS One 12:e0187779.

Wheeler AL, Teixeira CM, Wang AH, Xiong X, Kovacevic N, Lerch JP, McIntosh AR, Parkinson J, Frankland PW (2013) Identification of a functional connectome for long-term fear memory in mice. PLoS Comput Biol 9:e1002853.

Zhan J, Gurung S, Parsa SPK (2017) Identification of top-K nodes in large networks using Katz centrality. J Big Data 4 Available at: https://journalofbigdata.springeropen.com/articles/10.1186/s40537-017-0076-5.

Figure 1: Morris water task training alters memory ability in contextual fear conditioning. (**a**) Mice were trained on a repeated acquisition and performance testing variation of the MWT (*n*=6) or kept in conventional housing conditions (*n*=6) for 10 weeks. Afterwards all mice underwent contextual fear conditioning and a retention test 24 hours later. (**b**) During water maze training, the escape platform was moved every second day between 10 locations. After the 10th position, the platform was returned to the 1st position and the cycle was restarted. (**c**) Mean distance travelled in the water maze across each of the 20 locations. (**d**) During contextual fear memory retrieval, (**e**) there was no overall difference in freezing rates between the control group and the group which had underwent Morris Water Task training (Paired two-tailed t test; $P>0.05$). (**f**) However, mice who had underwent Morris Water Task training froze significantly more than control mice during the first half (minutes 0-3) of the test and less during the second half of the test (minutes 3-6; Two-Way ANOVA; Time × Treatment interaction: $F_{1,12}=15.86$, $P=0.0018$; MWT 0-3 – 3-6: $P<0.0001$). Data shown are mean±SEM when applicable.

Figure 2: Semi-automated pipeline for generating accurate regional c-Fos densities. (**a**) In the cell segmentation and tissue registration pipeline, tissue was sectioned, immuno-labeled, and mounted on slides prior to being imaged on a fluorescent slide scanning microscope. Images of labelled c-Fos and DAPI staining were then processed using *Ilastik* and *ImageJ* to generate binary c-Fos labels and a mask of evenly spaced grid points in the shape of the tissue sections. These binary images were then applied to plates from the *Allen Mouse Brain Atlas* which had been morphed to align with the tissue sections using *Whole Brain*, yielding regional c-Fos densities. (**b**) Examples of raw c-Fos^{+} cells in the BLA, CA1, DG, PVT, and RSC (top, L-R) and cells segmented using *Ilastik* (bottom). (**c**) A set of ROIs was quantified for validation. Automated *Ilastik* segmentation yielded cell counts within the 95% confidence intervals of counts acquired from trained independent experimenters in each of the aforementioned regions (Two-Way ANOVA; segmentation method factor:

$F_{1,15}$=0.09515, *P*=0.7620). (**d**) Cell counts collected using automated *Ilastik* processing were found to correlate highly with mean counts gathered through manual counting (*Pearson r*=0.9610, *P*<0.01). (**e**) Area approximations generated using the pipeline were correlated with areas acquired by tracing regions manually in *ImageJ* (*Pearson r*=0.9941, *P*=<0.0001). Data shown are mean ± SEM when applicable. (**f**) c-Fos quantification across the 98 brain regions of interest. Relative to the control group, c-Fos expression in the mice that had previously received Morris water task training was decreased in most brain regions and was higher in only a small number of regions.

Figure 3: Morris water task training alters global memory network topology. Pairwise correlation matrices for and binarized circle plots showing significant correlations between regions for control (a-b) and Morris water task trained (c-d) groups. See *Supplemental Table S1* for full list of regions. MWT training increased (**e**) network density. (**f**) The number of correlations involving each node at different correlation strength were normalized by network density to show that MWT training increased the proportion of the strongest connections in the network (Two-Way ANOVA; Pearson Threshold × Treatment interaction: $F_{3,776}$=3.904, *P*=0.0088; 0.8-1.0 CTRL - MWT: Tukey's *post hoc* test for multiple comparisons: *P*=0.0140). Data shown are mean±SEM when applicable.

Figure 4: Networks underlying contextual memory recall display small world-like properties. (**a**) Consistent with definitions of small world organization, in both control and MWT trained networks the majority of nodes were of a low degree. However, water maze training shifted the degree distribution and increased the number of highly connected nodes. (**b**) Also consistent with small world organization, both control and MWT trained networks showed equivalent global efficiency to random networks matched for degree distribution. Data shown are mean±95% confidence intervals. (**c**)

A third requirement for the classification of a small world organization is a higher clustering coefficient than a random network. Compared to random networks matched for degree distribution, both control and MWT trained networks showed heightened clustering ($F_{1,388}$=178.6, P<0.0001). Data analysis used Two-Way ANOVA. Data shown are mean±SEM

Figure 5: Morris water task training alters clustering patterns and increases network resiliency. Network plots of (**a**) control and (**b**) MWT trained networks with the giant component (GC) highlighted in each in the darker shade. Within these networks, there is very little difference in the size of the GC (**c**) and the number of components within the network (**d**) between conditions. (**e**) There was also no difference in the mean number of nodes per component (Two-tailed t test, P=0.6226). (**f**) Within the GC, there was an increase in the mean number of edges per node with MWT training (Two-tailed t test, P=0.0215). MWT training also made the (**g**) efficiency and (**h**) integrity of the GC more resilient to targeted node deletion. Relative to the control condition (**i**), MWT training (**j**) also increased Katz centrality of a subset of regions within the network. Note the difference in y-axis between panel I and J. Data shown are mean±SEM when applicable.

Figure 1

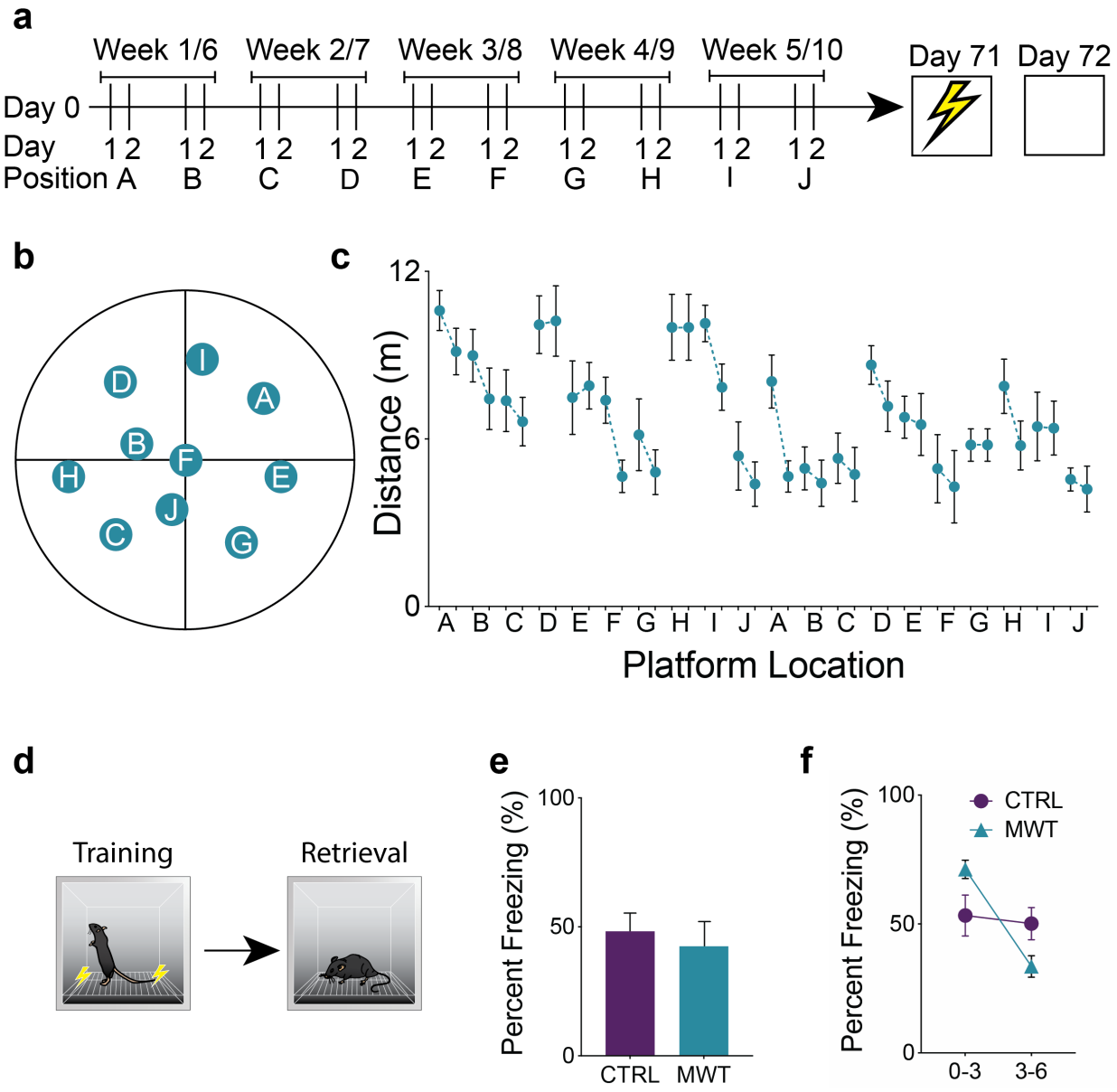
a
Week 1/6
Week 2/7
Week 3/8
Week 4/9
Week 5/10
Day 71
Day 72
Day 0
Day
Position
1 2
A B C D E F G H I J
b
c
Distance (m)
12
6
0
A B C D E F G H I J A B C D E F G H I J
Platform Location
d
Training
Retrieval
e
Percent Freezing (%)
100
50
0
CTRL
MWT
f
Percent Freezing (%)
100
50
0
CTRL
MWT
0-3
3-6

Figure 2

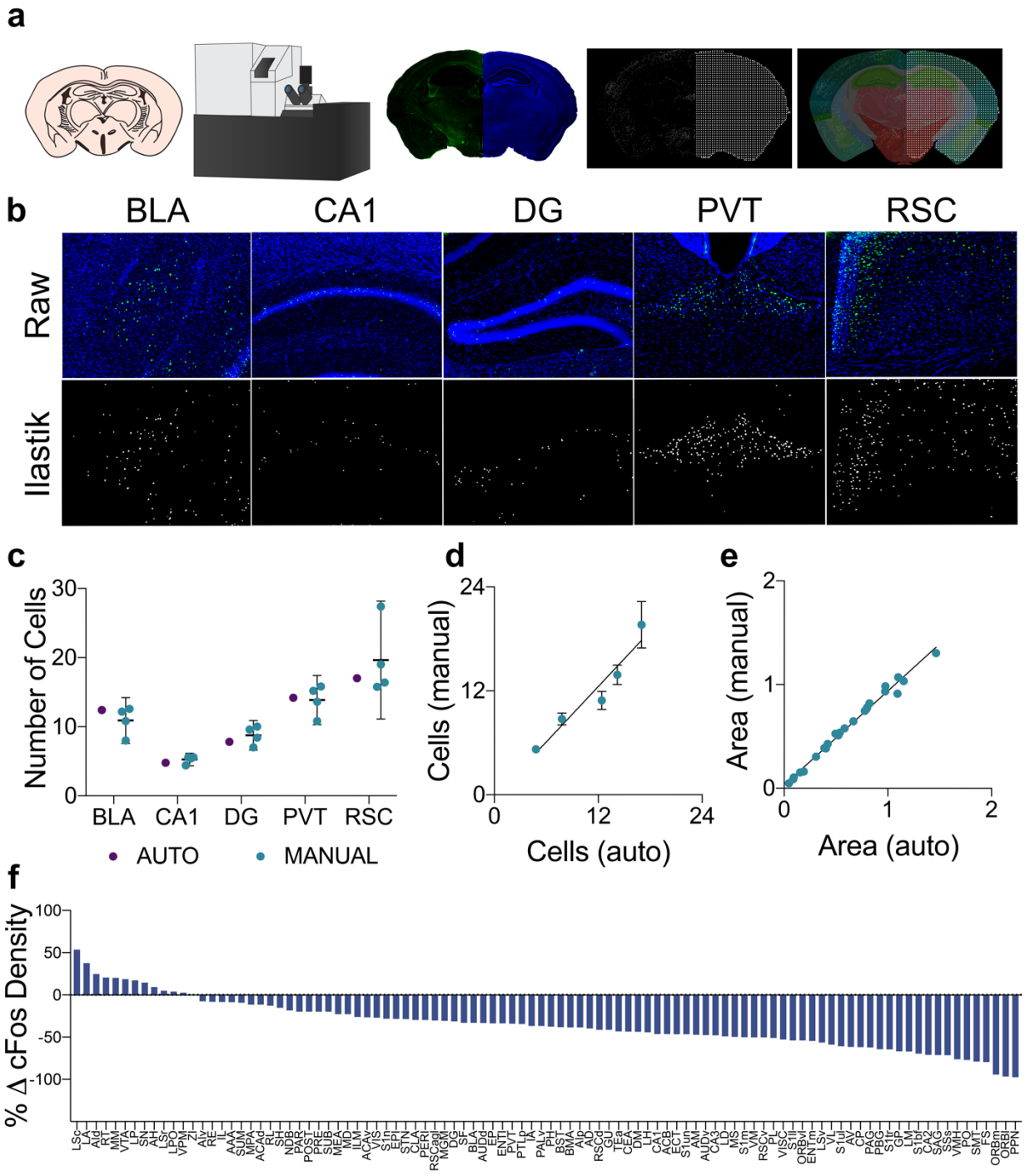
a
b
BLA
CA1
DG
PVT
RSC
Raw
Ilastik
c
Number of Cells
30
20
10
0
BLA
CA1
DG
PVT
RSC
AUTO
MANUAL
d
Cells (manual)
24
12
0
0
12
24
Cells (auto)
e
Area (manual)
2
1
0
0
1
2
Area (auto)
f
% Δ cFos Density
100
50
0
-50
-100

Figure 3

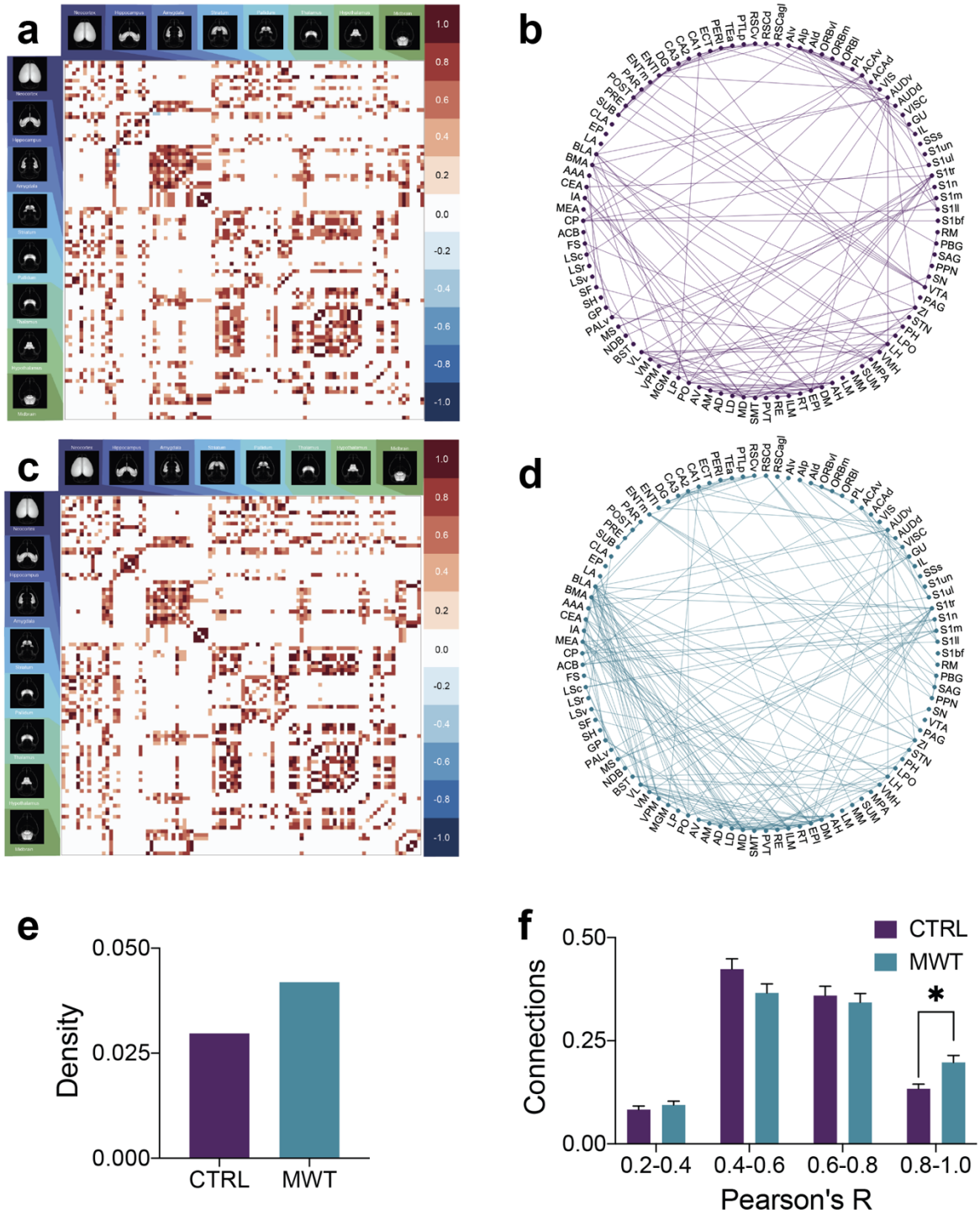
a
b
c
d
e
Density
0.050
0.025
0.000
CTRL
MWT
f
Connections
0.50
0.25
0.00
CTRL
MWT
*
0.2-0.4
0.4-0.6
0.6-0.8
0.8-1.0
Pearson's R

Figure 4

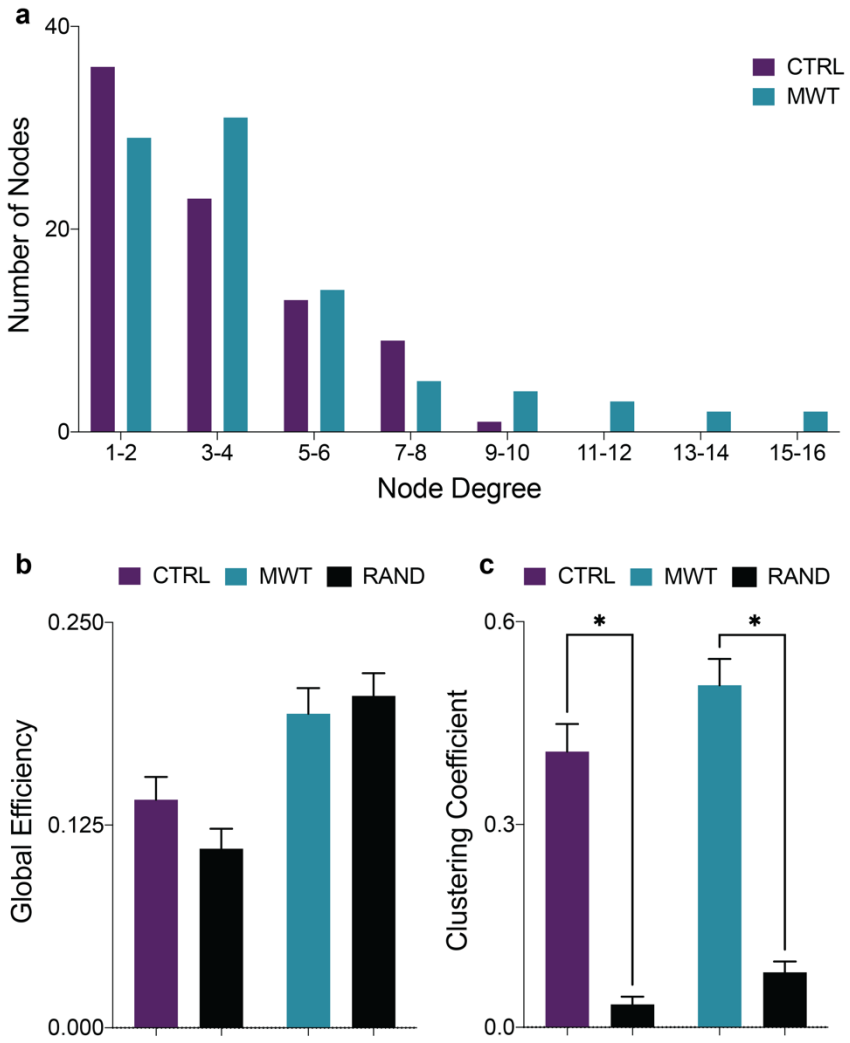
a
40
20
0
Number of Nodes
CTRL
MWT
1-2
3-4
5-6
7-8
9-10
11-12
13-14
15-16
Node Degree
b
CTRL
MWT
RAND
0.250
0.125
0.000
Global Efficiency
c
CTRL
MWT
RAND
0.6
0.3
0.0
Clustering Coefficient
*
*

Figure 5

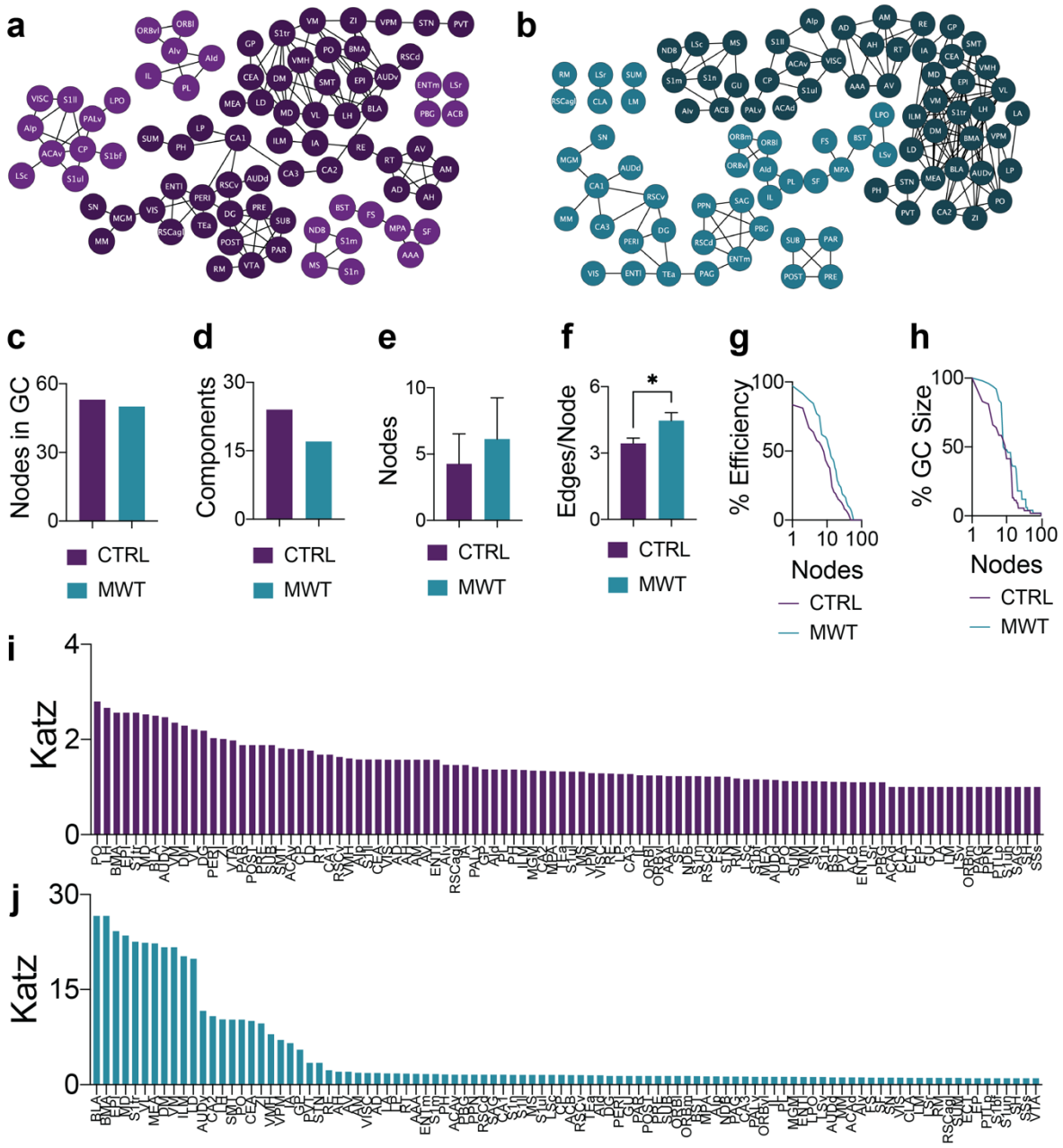
a
b
c
Nodes in GC
60
30
0
CTRL
MWT
d
Components
30
15
0
CTRL
MWT
e
Nodes
10
5
0
CTRL
MWT
f
Edges/Node
6
3
0
*
CTRL
MWT
g
% Efficiency
100
50
0
1
10
100
Nodes
CTRL
MWT
h
% GC Size
100
50
0
1
10
100
Nodes
CTRL
MWT
i
Katz
4
2
0
j
Katz
30
15
0